Nanoscale Compositional Modification in Co/Pd Multilayers for Controllable Domain Wall Pinning in Racetrack Memory

*Tianli Jin, Durgesh Kumar, Weiliang Gan, Mojtaba Ranjbar, Feilong Luo, Rachid Sbiaa, Xiaoxi Liu, Wen Siang Lew, and S. N. Piramanayagam**

In the era of social media, storage of information plays an important role. Magnetic domain wall memory devices are promising alternatives to hard disk drives for high-capacity storage. One of the challenges in making these devices for practical application is a precise control of domain wall displacement in nanowires. Researchers have extensively studied domain wall pinning based on topographical notches fabricated by lithography. However, scaling the domain wall memory to nanoscale requires better domain wall pinning strategies. In this letter, we demonstrate that the localized modification of magnetic properties in Co/Pd multilayer-based nanowires by ion implantation is an effective non-topographical approach to pin domain walls. First, by micromagnetic simulations, it is shown that the areas, where the composition is modified to tune the anisotropy and magnetization, act as domain wall pinning centers. Experimentally, from magnetization measurements and X-ray diffraction measurements at the thin film level, it is shown that the ion-implantation is effective in changing magnetic anisotropy. Devices have also been fabricated and, using Kerr images at different applied fields, it is shown that the domain walls are pinned at the B^+ ion-implanted regions. These results demonstrate that localized compositional modification using ion-implantation can pin domain walls precisely. The achieved results are useful toward realizing high-capacity information storage.

Domain wall (DW)-based devices such as racetrack memory have been proposed as promising candidates for high capacity, non-volatile information storage to replace hard disk drives.[1,2] In DW memory (DWM) with a perpendicular magnetic anisotropy (PMA), the domains with magnetization pointing up represent "1" and the regions with magnetization pointing down represent "0."[2,3] In order to read and write information, the DWs are moved by an electrical current which causes motion by the spin-transfer torque (STT) mechanism.[4–7] Spin Hall effect in heavy metal/ferromagnetic/insulator structures is another mechanism in which a torque is exerted by pure spin current.[8,9] In comparison to STT driving DW motion, pure spin-polarized current gives a high speed performance of DW devices.[10,11] The speed of DW motion in certain designs could reach km s^{-1}.[11] In order to increase the capacity of DWM, researchers proposed fabricating U-shape vertical nanowire to store data, like the trees planted in the forest. However, fabrication of such devices is challenging particularly for commercial purposes. The other structure is horizontal stripe shape, which suffers from the data storing overflowing issues because the two ends of nanowire cannot be connected. Zhang et al.[12] proposed a ring structure with DW ratchets, which could be utilized for addressing the data overflow issue without any additional overhead.

For DW-based devices, the propagation of DWs show a stochastic behavior. This stochastic manner was a significant challenge for magnetic recording community during the early stages of thin film recording media.[13,14] For this reason, the hard disk media industry moved from the use of continuous magnetic thin films to exchange-decoupled granular thin films, whereby the magnetization reversal by DW zig-zag motion was completely avoided.[15–17] Therefore, for reliable operation of ultra-high density DW devices, precise control of DW motion is important.[18–20]

In the studies carried out so far, the pinning sites for DW devices were fabricated by traditional lithography process by modifying the geometry, e.g., creation of notches or staggered

T. Jin, D. Kumar, W. Gan, M. Ranjbar, F. Luo, W. S. Lew, S. N. Piramanayagam
Division of Physics and Applied Physics
School of Physical and Mathematical Sciences
Nanyang Technological University
637371 Singapore, Singapore
E-mail: prem@ntu.edu.sg

R. Sbiaa
Department of Physics
Sultan Qaboos University
123 Muscat, Oman

X. Liu
Department of Electrical and Computer Engineering
Shinshu University
Nagano, Japan

The ORCID identification number(s) for the author(s) of this article can be found under https://doi.org/10.1002/pssr.201800197.

DOI: 10.1002/pssr.201800197

patterns in the ferromagnetic nanowire.[21–23] Exchange bias field to pin DWs has also been proposed in the past.[24] The pinning fields were introduced at the cross points by ferromagnetic wires and antiferromagnetic wires via exchange coupling between the two wires. Recently, we have proposed compositional modification using annealing-induced diffusion as a possible method to pin DWs.[25] There are also some reported studies about pinning DW by tuning anisotropy using focused ion beam irradiation.[26–32] In this letter, we propose an alternative approach, which is based on ion-implantation-induced local modification of magnetic properties for controlling DW displacement in Co/Pd multilayers-based DW devices. In comparison to focused ion beam technique, ion-implantation offers a variety of elements for selection and implantation through mask is easy to be adapted for mass manufacturing. At first, we carried out micromagnetic simulations to investigate if DWs could be pinned by local compositional variation. Secondly, we carried out experimental investigations to understand the effects of ion-implantation on the magnetic and structural properties of Co/Pd multilayers. As a next step, we demonstrated DW pinning in the fabricated devices using the proposed method. Finally, we show STT-driven DW motion and effective pinning by simulation results. The results highlighted in this report are useful in the development of DW memory devices.

Simulation: We first studied the DW position as a function of time using Mumax3. The time-dependent magnetization dynamics under applying current is expressed by using the extended Landau–Lifshitz–Gilbert (LLG) equation, which has been taken into account both the adiabatic and non-adiabatic terms of STT[33,34]

$$\frac{d\boldsymbol{M}}{dt} = -\gamma_0 \boldsymbol{H}_{\text{eff}} \times \boldsymbol{M} + \frac{a}{M_s}\boldsymbol{M} \times \frac{d\boldsymbol{M}}{dt} + \boldsymbol{\Gamma}_{\text{STT}} \quad (1)$$

Here γ_0 is the Gilbert gyromagnetic ratio, a is the Gilbert damping coefficient, and $\boldsymbol{M}$ is the magnetization. The $\boldsymbol{H}_{\text{eff}}$ in Equation (1) is the effective field acting on the local magnetization $\boldsymbol{M}$ which includes perpendicular anisotropy and magnetostatic interaction. The spin transfer torque $\boldsymbol{\Gamma}_{\text{STT}}$ generated by current can be expressed by the following relation

$$\boldsymbol{\Gamma}_{\text{STT}} = -(a_J/M_s)\boldsymbol{M} \times (\boldsymbol{M} \times \boldsymbol{P}) - b_J(\boldsymbol{M} \times \boldsymbol{P}) \quad (2)$$

where $\boldsymbol{P}$ is the spin polarization vector, a_J is the strength of anti-damping torque effect, and b_J is the strength of field-like torque effect.

Two types of nanowire devices of Co/Pd multilayer structure (type A: with length of 128 nm, width of 16 nm, and the thickness of 2 nm and type B: length of 5120 nm, width of 1280 nm, and thickness of 10 nm) were used in the simulation. **Figure 1** shows the simulation results of type A structures. We chose the material properties of Co/Pd multilayers at the unimplanted areas, viz., $M_s = 400$ emu/cc and magnetic anisotropy energy $K_u = 5\times10^6$ erg/cc and defined the areas where compositional modification were carried out to have a lower saturation magnetization M_s (200 emu/cc) and lower magnetic anisotropy energy $K_u = 1 \times 10^6$ erg/cc. All through simulation, a discretization of $2 \times 2 \times 2\,\text{nm}^3$ is used which is sufficiently smaller than the exchange length.[35]

Figure 1(a1–a3) show DW propagation in nanowires without domain wall pinning sites. In these wires, M_s and K_u are uniform throughout the length, representing a wire with no implantation-induced local modification. When a current was sent with a density of $5 \times 10^{10}\,\text{A m}^{-2}$, the domain walls propagated to the end of nanowire without stopping. The domain wall velocity was found to be $8\,\text{m s}^{-1}$.[36] Figure 1(b1–b3) illustrate the scenario for the nanowires with modified regions. It can be noticed that the DW stopped at the region and became widen. When the spin-polarized current was increased to $2 \times 10^{11}\,\text{A m}^{-2}$, DW was depinned and moved to the end of nanowire. Therefore, the simulation results indicate that the proposed scheme has the potential to pin DWs in a controllable manner. Detailed

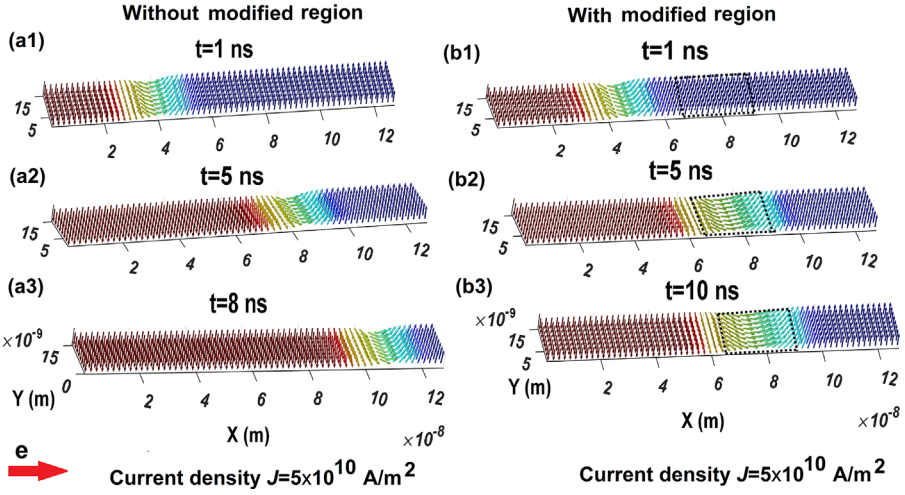

Figure 1. Micromagnetic simulation studies of DW propagation in two magnetic nanowires (a) without pinning sites and (b) with periodic pinning sites which have different magnetic properties from other regions. Parts (a1–a3) depict the domain wall position at different times in nanowires without pinning sites. Parts (b1–b3) depict the domain wall position at different times in nanowires where local modification of magnetic properties were carried out to create pinning sites. A spin current with a current density of $5 \times 10^{10}\,\text{A m}^{-2}$ was used to move DWs. The dashed boxes show the modified area.[35]

description of further simulation studies are presented at the end of this letter.

Results and Discussion: In order to demonstrate the pinning of DWs by the compositionally modified areas experimentally, we used a Co/Pd multilayer films with a perpendicular magnetic anisotropy. N multilayers films with different thickness were deposited using DC magnetron sputtering system. As shown in **Figure 2**(a), the films consist of Si (SiO_2)/Ta (5 nm)/Cu (5 nm)/Pd (3 nm)/[Co (0.3 nm)/Pd (0.8 nm)]$_N$/Ta (5 nm), where N (=5, 10, and 15) indicates the repeating cycles in each film. The magnetic properties of each film were characterized by alternating gradient force magnetometer (AGFM) along the out of plane (OOP) and in-plane (IP) directions. The characterized magnetic hysteresis loops (M–H) are shown in Figure 2(b). The rectangular loops for [Co/Pd]$_{5,10,15}$ bilayers indicate the presence of a strong PMA in each film, as seen from the OOP measurement. The inset in Figure 2(b) shows the strong perpendicular magnetic anisotropy according to the different behavior of OOP and in-plane hysteresis loops of Co/Pd multilayers sample with $N = 15$. The wafer with deposited film were then diced and divided into two different groups to compare the magnetic properties with and without ion-implantation. A 10 keV B^+ implantation was carried out at a fluence of 5×10^{15} ions/cm^2 to achieve the compositional modification on one group of the films.

The magnetic properties of the B^+ ion-implanted samples were characterized by AGFM along the OOP direction and polar Kerr imaging microscopy after ac demagnetization in a OOP field. The hysteresis loops are shown in **Figure 3**, where the OOP hysteresis loops characterized from the unimplanted samples are included for comparison. Changes of the OOP hysteresis loops were observed from the two group samples, as shown in Figure 3(a, d, and g). The hysteresis loops of implantation [Co/Pd]$_{5,10}$ samples, which vary from that of the non-implantation samples, indicate that the implanted [Co/Pd]$_{5,10}$ samples have no PMA and the magnetizations lie in-plane. The same results can be confirmed from the domain images. All the unimplanted samples show micro-size stripe domains with a strong contrast, which are typical of films with a PMA, as shown in Figure 3(b and e), but after B^+ implantation, the stripe domains disappear, as shown in Figure 3(c and f). The PMA of the implanted sample with $N = 15$ decreases, compared to the unimplanted ones, as shown in Figure 3(g). The stripe domains in $N = 15$ sample becomes weaker after implantation, as compared in Figure 3(h) and (i). In general, the anisotropy decreases for the B^+ implanted samples. We propose that the decline is attributed to the change of Co/Pd interfaces caused by the implantation, as the PMA arises from Co and Pd interface.[37–41]

X-ray diffraction (XRD) measurements were carried out on unimplanted and implanted samples to validate our hypothesis. The measurement results are shown in **Figure 4**. For the unimplanted case, the samples show a peak at 40.8, 41, and 41.1° for $N = 5$, 10, and 15, respectively. The peaks follow the widely reported behavior that the peak position depends on the relative thickness of Co and Pd layers in Co/Pd multilayer systems.[18,19] Since pure Pd (111) exhibits a peak at around 40.8° and pure Co (111) exhibits a peak at around 44.4°, the Co/Pd multilayers exhibit a peak in between these two angles, depending on the relative thickness of Co and Pd. The peak position also varies with the number of bilayers. In the case of $N = 15$, there are more Co layers in comparison to the sample with $N = 5$ and hence the peak shifts toward the higher angles (closer toward the Co (001) peak). For the B^+ implantation group, the peak shifts toward lower 2θ values, compared to the unimplanted group. This implies that the the Co and Pt interfaces of B^+ implanted samples vary from those of unimplanted samples. The shift magnitude is 0.59, 0.45, and 0.32° for $N = 5$, 10, and 15, which indicates that it has an inverse dependence on the value of N. The shift is partially attributed to the intermixing of Co and Pd caused by the implantation as verified later by transport of ions in matter (TRIM) simulation. Due to the intermixing, for small values of N, layers that had predominantly Co become mixed with Pd atoms due to ion-implantation. As a result, the peak shifts toward lower values of 2θ. The B^+ occupation in the interstitial positions, which can result in further shift toward lower 2θ values, also contributes to the shift. However, the shift due to B^+ occupation is not significant for samples with $N = 15$, because the penetration of B^+ is not deep.[37]

In order to understand the intermixing of Co and Pd, we carried out TRIM simulation of the distribution of Co and Pd atoms displaced from their initial positions.[37,42] The diffusion between Co and Pd atoms is clear for $N = 5$ and 10 as shown in **Figure 5**. For $N = 15$, the diffusion between Co and Pd is not significant. This inter-diffusion corroborates with the reduction in the magnetic anisotropy and the XRD results.

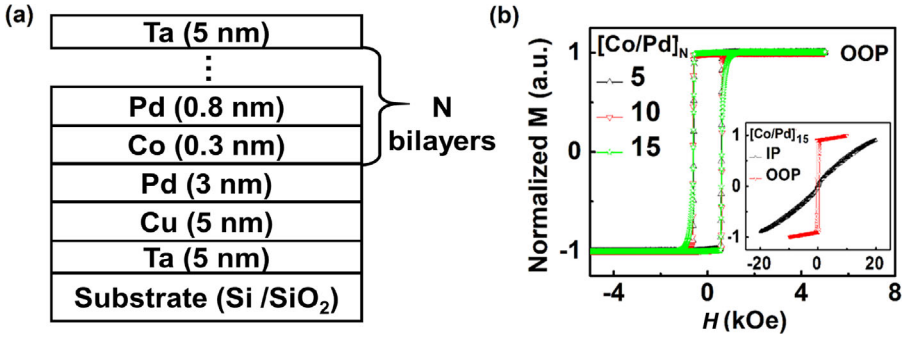

Figure 2. a) Schematic illustration of a sample stack structure used in this study and b) out-of-plane (OOP) hysteresis loops of Co/Pd multilayers with different values of N. The inset shows the in-plane (IP) and OOP hysteresis loops of [Co/Pd]$_{15}$.

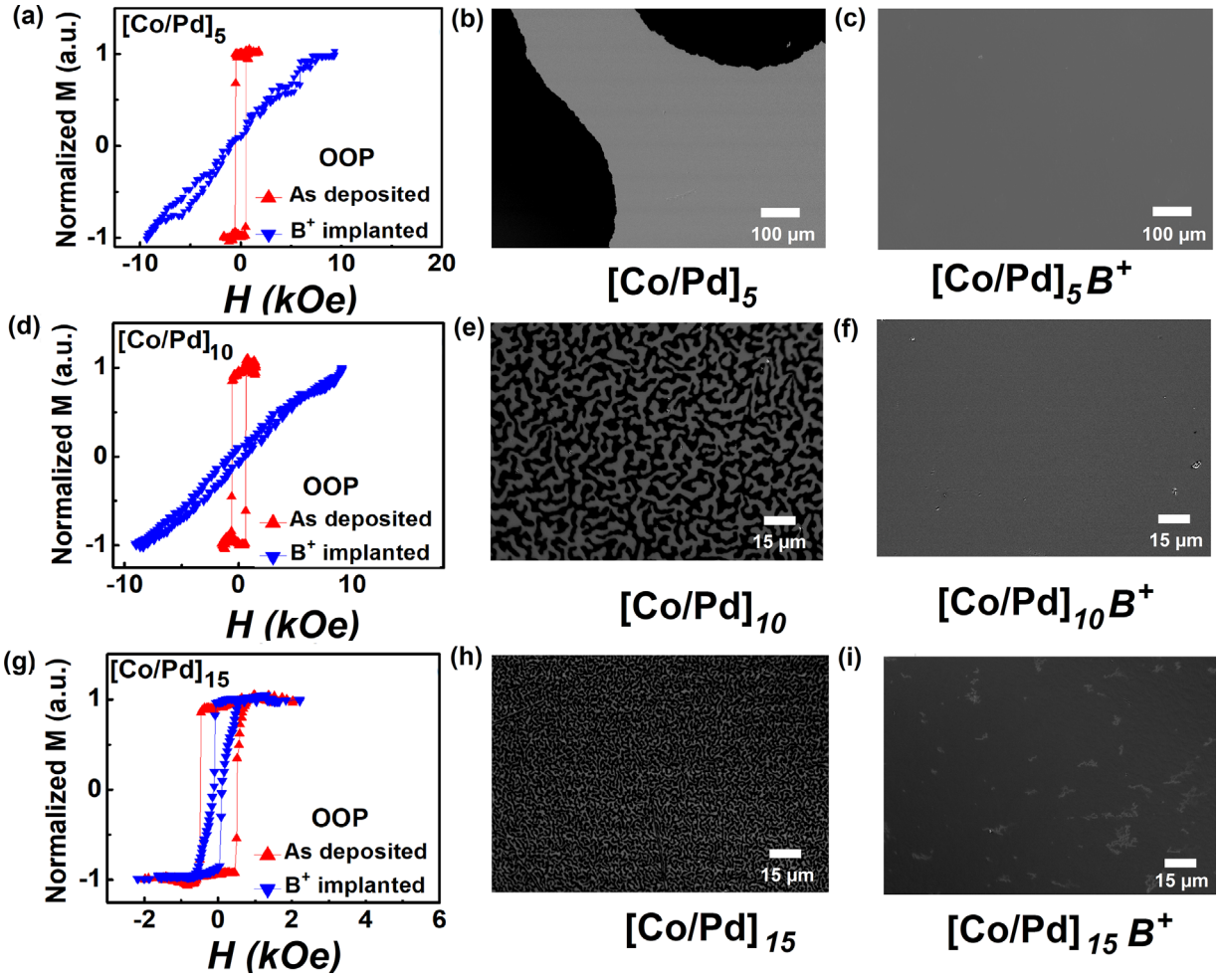

Figure 3. a,d,g) Hysteresis loops of $[Co/Pd]_N$ multilayers with different values of *N*, with and without implantation. Domain images of $[Co/Pd]_N$ multilayers with different values of *N*, (b, e, and h) before implantation and (c, f, and i) after implantation. The black and gray regions represent magnetization in two different orientations (into the paper and out-of-paper, for example).

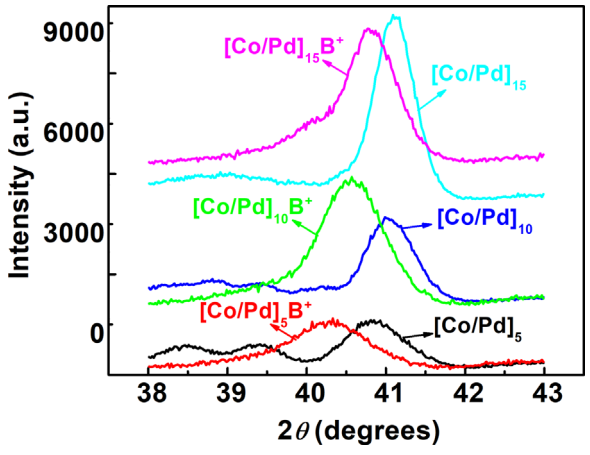

Figure 4. XRD peaks of samples with different values of *N*, with and without B^+ implantation.

The investigations so far indicate that the B^+ implantation causes the changes in the magnetic and structural properties of Co/Pd multilayers. In order to demonstrate that such modified areas act as pinning centers in experiments, a $[Co/Pd]_{10}$ nanowire device with localized B^+ implantation was fabricated by E-beam lithography and ion-beam etching. The fabrication process can be seen in Sample Preparation section. Kerr imaging system was used to observe the DW nucleation and motion. Initially, the nanowire device was magnetized to saturation to eliminate DWs. Kerr image shows gray regions (**Figure 6**(a)), which indicates that there are no DW in the device after saturation. Later, a 10 mA pulse current with 1 ms width was sent through the injection line to give rise to Oersted field to nucleate DWs in the wire devices.[43,44] As shown by Kerr image in Figure 6(b), two magnetic domains which are in black were generated beside the cross-bar. (The reason for the small domain at the right side is not clear). The reversal magnetic field was increased gradually. At an external magnetic field of 900 Oe, the DW moved to the pinning center, as evidenced by the expansion of the black region to the position where the B^+ implantation is

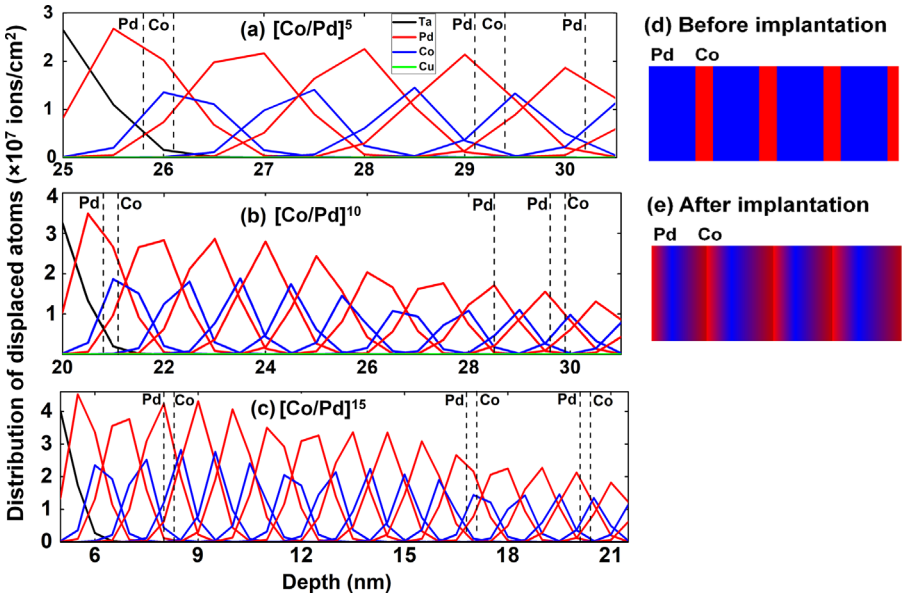

Figure 5. The distribution of displaced atoms (obtained from TRIM simulation) of Co and Pd after B^+ implantation (a) for $N = 5$, (b) for $N = 10$, and (c) for $N = 15$ bilayers. The dashed lines indicate the middle portion of the Co and Pd layers before ion implantation. The Co and Pd layers were assumed to be sharp before implantation, as shown in illustration (d). After implantation, the atoms are diffused as illustrated in (e).

located. The black region does not expand further when the applied field was increased to 910 Oe, which indicates that the DW is pinned at this position. This fact implies that the pinning center formed by B^+ implantation in this region is effective. When the external magnetic field was increased to 920 Oe, the black region moved across the implantation position and spread to the end of the device. Hence, it can be concluded that the implantation region acts as a pinning center to stabilize the DWs, and the pinning and depinning field are close to 900 and 920 Oe, respectively. It may be argued that the geometrical modification around the small cross-bar due to ion-implantation is a possible cause of pinning. However, we believe that this effect is negligible, as the depinning field is much larger (920 Oe) than observed in the case of geometrical modification, such as notches (100 Oe).[45–47]

In order to understand how effective would be the pinning in the case of STT-induced DW motion, we carried out further micromagnetic simulations. For this study, we used type B structures, which resemble our experimental devices closely. **Figure 7** shows the values of anisotropy constant (K_u) and the saturation magnetization (M_s) of the implanted regions. When a current was sent through the device, the domain walls moved and got pinned in the regions with a lower K_u or M_s. When the current density was increased further, the domain walls got depinned and moved further. The current density associated with depinning J_{dep} is shown in the table and in the graph. It can be noticed from the table that the depinning current density increases when both K_u and M_s decreases (diagonal direction of the table). In the case of ion-implantation, both K_u and M_s are expected to decrease. So, this trend is a clear indication that the

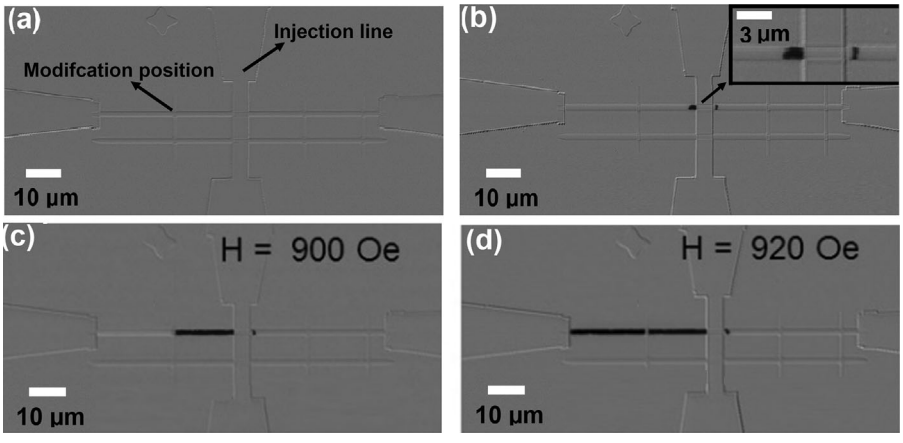

Figure 6. a) Kerr image of the nanowire device in the saturation state. b) DW nucleation at the crossbar after the application of the current along injection line and (c and d) the DW propagation by applying different magnetic fields along perpendicular direction.

(a)

J_{dep} (×10^{11} A/m^2)

K_u \ M_s	400 (emu/cc)	300 (emu/cc)	200 (emu/cc)
5×10^6 (erg/cc)	No Pinning	6.8	12
3×10^6 (erg/cc)	5.2	6.4	7.2
1×10^6 (erg/cc)	16	5.8	7.8

(b)

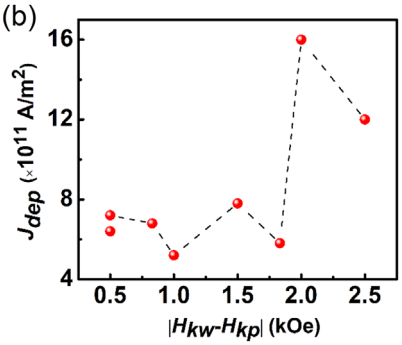

Figure 7. a) Tabulation of depinning current density J_{dep} for pinning regions with various values of K_u and M_s. b) Plot of depinning current density J_{dep} for pinning regions with various values of K_u and M_s.

ion-implantation-induced local modification is a good technique to pin the domain walls. The graph shows the trend of J_{dep} as a function of Mod (H_{kw}–H_{kp}) where H_{kw} is the anisotropy field of the wire and H_{kp} is the anisotropy field of the pinning region, obtained from the relation $H_k = 2K_u/M_s$. In general, an increase in the value of J_{dep} associated with an increase in the difference between H_{kw} and H_{kp} is noticed. These results further confirm that the ion-implantation induced changes in local magnetic properties can help in forming pinning centers.

In conclusion, the DW pinning method using compositional modifications by ion implantation has been investigated. This method has been validated by simulations and experiments. We have observed that B^+ implantation can reduce the anisotropy of the Co/Pd multilayers and change the magnetization from perpendicular to in-plane direction. In $[Co/Pd]_{10}$ nanowire study, the pinning field can be as high as 920 Oe.

Experimental Section

Sample Preparation: Thin film stack of Ta (5 nm)/Cu (5 nm)/Pd (3 nm)/[Co (0.3 nm)/Pd (0.8 nm)]$_N$/Ta (5 nm), where $N = 5$, 10, and 15, were deposited on thermally oxidized silicon substrates via DC magnetron sputtering at room temperature. The bilayers Co and Pd were grown at the DC power of 40 W and the deposition rate of Co and Pd is 0.4 and 0.357 nm s^{-1}, respectively.

The Co/Pd multilayers-based microwires fabrication was carried out by E-beam lithography (EBL). The Co/Pd multilayers thin film was patterned to 1 μm wires under 20 keV voltage and 7 μm aperture. After E-beam exposure, Ar ion-milling was done to eliminate the unwanted film. The resist PMMA with the thickness of 200 nm over Co/Pd multilayers-based microwires were exposed under 10 keV voltage and 30 μm aperture. After developing, B^+ ions were implanted in the holes of the resist. The B^+ ions were with the energy of 10 keV which were at a fluence of 5×10^{15} ions/cm^2. After this, the DW injection line and electrode pads were exposed under 20 keV and 120 μm aperture and after developing, Ti (10 nm)/Au (80 nm)/Ti (10 nm) were deposited in order to inject DW and cause DW motion by applying pulse current.

Sample Characterization: Normalized magnetic hysteresis loops (M–H) of Co/Pd multilayers thin film along IP and OOP directions were carried out at room temperature by using AGFM with the magnetic sweeping from −20 to 20 kOe. XRD with Cu-K_α source was used for the structural analysis of the samples. TRIM program was used to simulate the distribution of host atoms after B^+ implantation. Domain images were carried out by using Polar Kerr imaging technique after ac demagnetization along OOP direction. In the demagnetization process, the magnetic field was cycled to zero with the step of 25 Oe decreasing from 4500 Oe, producing a demagnetized state. Direct observation of the DW pinning process was carried out using Polar Kerr imaging technique.

Acknowledgments

The authors gratefully acknowledge Nanyang Technological University Start-Up Grant and AcRF-Tier 1 grant RG163/15 for the funding of this research. The authors would like to acknowledge Calvin Ang Ching Ian for his help in Kerr microscopy measurement.

Conflict of Interest

The authors declare no conflict of interest.

Keywords

Co/Pd multilayers, compositional modification, domain wall memory, domain wall pinning, ion implantation

Received: April 21, 2018
Revised: July 30, 2018
Published online:

[1] J. S. Meena, S. M. Sze, U. Chand, T. Y. Tseng, *Nanoscale Res. Lett.* **2014**, *9*, 526.
[2] Z. T. Diao, Z. J. Li, S. Y. Wang, Y. F. Ding, A. Panchula, E. Chen, L. C. Wang, Y. M. Huai, *J. Phys.: Condens. Matter* **2007**, *19*, 165209.
[3] R. Sbiaa, H. Meng, S. N. Piramanayagam, *Phys. Status Solidi RRL* **2011**, *5*, 413.
[4] J. Slonczewski, *J. Magn. Magn. Mater.* **1996**, *159*, L1.
[5] D. Chiba, G. Yamada, T. Koyama, K. Ueda, H. Tanigawa, S. Fukami, T. Suzuki, N. Ohshima, N. Ishiwata, Y. Nakatani, T. Ono, *Appl. Phys. Express* **2010**, *3*, 073004.

[6] R. Sbiaa, S. N. Piramanayagam, *Phys. Status Solidi RRL* **2017**, *11*, 1700163.
[7] S. Bhatti, R. Sbiaa, A. Hirohata, H. Ohno, S. Fukami, S. N. Piramanayagam, *Mater. Today* **2017**, *20*, 530.
[8] O. Boulle, G. Malinowski, M. Kläui, *Mater. Sci. Eng. R, Rep*. **2011**, *72*, 159.
[9] S. Emori, U. Bauer, S. M. Ahn, E. Martinez, G. S. Beach, *Nat. Mater.* **2013**, *12*, 611.
[10] S. Parkin, S. H. Yang, *Nat. Nanotechnol*. **2015**, *10*, 195.
[11] S. H. Yang, K. S. Ryu, S. Parkin, *Nat. Nanotechnol*. **2015**, *10*, 221.
[12] Y. Zhang, X. Y. Zhang, J. T. Hu, J. Nan, Z. Y. Zheng, Z. Z. Zhang, Y. G. Zhang, N. Vernier, D. Ravelosona, W. S. Zhao, *Sci. Rep*. **2016**, *6*, 23164.
[13] S. N. Piramanayagam, *J. Appl. Phys*. **2007**, *102*, 011301.
[14] Y. H. Tang, J. G. Zhu, *IEEE Trans. Magn*. **2007**, *43*, 2139.
[15] S. N. Piramanayagam, B. Varghese, Y. Yang, W. K. Lee, H. K. Tan, *J. Appl. Phys*. **2014**, *115*, 243901.
[16] D. Weller, G. Parker, O. Mosendz, A. Lyberatos, D. Mitin, N. Y. Safonova, M. Albrecht, *J. Vac. Sci. Technol. B* **2016**, *34*, 060801.
[17] N. Xiao, B. Yang, J. S. Wang, S. Li, Y. P. Ren, G. W. Qin, *Rare Metals* **2016**, *35*, 463.
[18] M. Albert, M. Franchin, T. Fischbacher, G. Meier, H. Fangohr, *J. Phys.: Condens. Matter* **2012**, *24*, 024219.
[19] M. Y. Im, L. Bocklage, P. Fischer, G. Meier, *Phys. Rev. Lett*. **2009**, *102*, 147204.
[20] A. Vogel, S. Wintz, J. Kimling, M. Bolte, T. Strache, M. Fritzsche, M. Y. Im, P. Fischer, G. Meier, J. Fassbender, *IEEE Trans. Magn*. **2010**, *46*, 1708.
[21] S. S. Parkin, X. Jiang, C. Kaiser, A. Panchula, K. Roche, M. Samant, *Proc. IEEE* **2003**, *91*, 661.
[22] R. Sbiaa, M. Al Bahri, *J. Magn. Magn. Mater.* **2016**, *411*, 113.
[23] M. Al Bahri, R. Sbiaa, *Sci. Rep*. **2016**, *6*, 28590.
[24] A. J. V. I. Polenciuc, D. A. Allwood, T. J. Hayward, G. Vallejo-Fernandez, K. O'Grady, A. Hirohata, *Appl. Phys. Lett*. **2014**, *105*, 162406.
[25] T. L. Jin, M. Ranjbar, S. K. He, W. C. Law, T. J. Zhou, W. S. Lew, X. X. Liu, S. N. Piramanayagam, *Sci. Rep*. **2017**, *7*, 16208.
[26] J. H. Franken, M. Hoeijmakers, R. Lavrijsen, H. J. Swagten, *J. Phys.: Condens. Matter* **2012**, *24*, 024216.
[27] T. Gerhardt, A. Drews, G. Meier, *J. Phys.: Condens. Matter* **2012**, *24*, 024208.
[28] J. A. King, A. Ganguly, D. M. Burn, S. Pal, E. A. Sallabank, T. P. A. Hase, A. T. Hindmarch, A. Barman, D. Atkinson, *Appl. Phys. Lett*. **2014**, *104*, 242410.
[29] D. M. Burn, D. Atkinson, *J. Appl. Phys*. **2014**, *116*, 163901.
[30] J. H. Franken, M. Hoeijmakers, R. Lavrijsen, J. T. Kohlhepp, H. J. M. Swagten, B. Koopmans, E. van Veldhoven, D. J. Maas, *J. Appl. Phys*. **2011**, *109*, 07D504.
[31] J. H. Franken, M. A. J. van der Heijden, T. H. Ellis, R. Lavrijsen, C. Daniels, D. McGrouther, H. J. M. Swagten, B. Koopmans, *Adv. Funct. Mater.* **2014**, *24*, 3508.
[32] R. Lavrijsen, G. Malinowski, J. H. Franken, J. T. Kohlhepp, H. J. M. Swagten, B. Koopmans, M. Czapkiewicz, T. Stobiecki, *Appl. Phys. Lett*. **2010**, *96*, 022501.
[33] A. V. Khvalkovskiy, K. A. Zvezdin, Y. V. Gorbunov, V. Cros, J. Grollier, A. Fert, A. K. Zvezdin, *Phys. Rev. Lett*. **2009**, *102*, 067206.
[34] S. Zhang, Z. Li, *Phys. Rev. Lett*. **2004**, *93*, 120201.
[35] R. Sbiaa, S. N. Piramanayagam, *Appl. Phys. A* **2014**, *114*, 1347.
[36] S. Gadetsky, *IEEE Trans. Magn*. **1995**, *31*, 3361.
[37] N. Gaur, K. K. M. Pandey, S. L. Maurer, S. N. Piramanayagam, R. W. Nunes, H. Yang, C. S. Bhatia, *J. Appl. Phys*. **2011**, *110*, 083917.
[38] N. Gaur, S. N. Piramanayagam, S. L. Maurer, R. W. Nunes, S. Steen, H. Yang, C. S. Bhatia, *J. Phys. D: Appl. Phys*. **2011**, *44*, 365001.
[39] Ikhtiar, K. Mukaiyama, S. Kasai, K. Hono, *Appl. Phys. Lett*. **2017**, *111*, 202407.
[40] A. Krichevsky, A. Lavrenov, N. Amos, B. Hu, K. Taylor, S. Khizroev, *J. Nanoelectron. Optoelectron*. **2008**, *3*, 274.
[41] B. Tudu, A. Tiwari, *Vacuum* **2017**, *146*, 329.
[42] N. Gaur, S. Kundu, S. N. Piramanayagam, S. L. Maurer, H. K. Tan, S. K. Wong, S. E. Steen, H. Yang, C. S. Bhatia, *Sci. Rep*. **2013**, *3*.
[43] S. H. Li, S. Goolaup, J. Kwon, F. L. Luo, W. L. Gan, W. S. Lew, *Sci. Rep*. **2017**, *7*, 972.
[44] M. Ramu, S. Goolaup, W. L. Gan, S. Krishnia, G. J. Lim, W. S. Lew, *Appl. Phys. Lett*. **2017**, *110*, 162402.
[45] L. K. Bogart, D. Atkinson, K. O'Shea, D. McGrouther, S. McVitie, *Phys. Rev. B* **2009**, *79*, 054414.
[46] Y. Gao, B. You, X. Z. Ruan, M. Y. Liu, H. L. Yang, Q. F. Zhan, Z. Li, N. Lei, W. S. Zhao, D. F. Pan, J. G. Wan, J. Wu, H. Q. Tu, J. Wang, W. Zhang, Y. B. Xu, J. Du, *Sci. Rep*. **2016**, *6*, 31908.
[47] Y. Gao, B. You, H. L. Yang, Q. F. Zhan, Z. Li, N. Lei, W. S. Zhao, J. Wu, H. Q. Tu, J. Wang, L. J. Wei, W. Zhang, Y. B. Xu, J. Du, *AIP Adv.* **2016**, *6*, 105301.